



Published in final edited form as:

Nat Chem Biol. 2020 August ; 16(8): 904–911. doi:10.1038/s41589-020-0548-3.

Pyridoxal-5'-Phosphate-Dependent Alkyl Transfer in Nucleoside Antibiotic Biosynthesis

Zheng Cui[†], Jonathan Overbay[†], Xiachang Wang^{‡,§}, Xiaodong Liu[†], Yinan Zhang^{‡,§},
Minakshi Bhardwaj[†], Anke Lemke[⊥], Daniel Wiegmann[⊥], Giuliana Niro[⊥], Jon S. Thorson^{†,‡},
Christian Ducho[⊥], Steven G. Van Lanen^{*,†}

[†]Department of Pharmaceutical Sciences, College of Pharmacy, University of Kentucky, Lexington, Kentucky 40536, United States

[‡]Center for Pharmaceutical Research and Innovation, College of Pharmacy, University of Kentucky, Lexington, Kentucky 40536, United States

[§]Jiangsu Key Laboratory for Functional Substance of Chinese Medicine, School of Pharmacy, Nanjing University of Chinese Medicine, Nanjing 210023, People's Republic of China

[⊥]Department of Pharmacy, Pharmaceutical and Medicinal Chemistry, Saarland University, Campus C2 3, 66123 Saarbrücken, Germany

Abstract

Several nucleoside antibiotics are structurally characterized by a 5''-amino-5''-deoxyribose (ADR) appended via a glycosidic bond to a high-carbon sugar nucleoside, (5',S,6',S)-5'-C-glycyluridine (GlyU). GlyU is further modified with an *N*-alkylamine linker, the biosynthetic origins of which have yet to be established. By using a combination of feeding experiments with isotopically labeled precursors and characterization of recombinant proteins from multiple pathways, the biosynthetic mechanism for *N*-alkylamine installation for ADR-GlyU-containing nucleoside antibiotics has been uncovered. The data reveal *S*-adenosyl-L-methionine (AdoMet) as the direct precursor of the *N*-alkylamine, but unlike conventional AdoMet- or decarboxylated AdoMet-dependent alkyltransferases, the reaction is catalyzed by a pyridoxal-5'-phosphatase (PLP)-dependent aminobutyryltransferase (ABTase) using a stepwise γ -replacement mechanism that couples γ -elimination of AdoMet with aza- γ -addition onto the disaccharide alkyl acceptor. In addition to utilizing a conceptually different strategy for AdoMet-dependent alkylation, the newly discovered ABTases require a phosphorylated disaccharide alkyl acceptor, revealing a cryptic intermediate in the biosynthetic pathway.

Users may view, print, copy, and download text and data-mine the content in such documents, for the purposes of academic research, subject always to the full Conditions of use:http://www.nature.com/authors/editorial_policies/license.html#terms

*To whom correspondence should be addressed. Tel: 1-859-323-6271; svanlanen@uky.edu.

Author contributions

Z. C. and J. O. performed and analyzed the data for cloning, heterologous expression, and protein functional assignments and biochemical characterization. Z. C., X. W., and M. B. performed MS and NMR spectroscopy of enzymatic products and analyzed the respective data. X. L., Y. Z., A. L., D. W., and G. N. performed the chemical synthesis and analyzed the respective data. Z. C., J. S. T., C. D., and S. G. V. L. conceived the study, directed and planned the research, analyzed the data, and wrote the paper.

Competing interests. The authors declare no competing interests.

Keywords

Biosynthesis; antibiotic; nucleoside; γ -replacement; aza-addition; pyridoxal-5'-phosphate; *S*-adenosyl-L-methionine

Introduction

Nucleoside antibiotics are a large family of natural products that have diverse biological activity and frequently complex structures requiring unparalleled biochemistry for their synthesis. Many nucleoside antibiotics inhibiting translocase I (TL1) involved in peptidoglycan synthesis have recently been discovered¹, and several biochemical studies have already established numerous examples of the latter². One group of TL1 inhibitors is structurally characterized by a disaccharide core consisting of a 5''-amino-5''-deoxyribose (ADR) linked to a high-carbon sugar nucleoside, (5' *S*,6' *S*)-5'-*C*-glycyluridine (GlyU), represented by FR-900493 (**1**), caprazamycin B (**2**), A-90289 B (**3**), sphaerimicin A (**4**), and muraymycin D1 (**5**) and D2 (**6**) (Fig. 1)³⁻⁷. The structures of **1-5** diverge outside of the shared ADR-GlyU disaccharide core, with each appended via a 6'-*N*-alkylamine linker to a unique glycosylated fatty acid, polyketide, or peptide moiety. Compound **1**, the structurally simplest of this nucleoside group with antibiotic activity, is modified with a methylated aminopropyl (C₃N) group attached to the ADR-GlyU disaccharide core. Structural inspection of **5** reveals the identical C₃N group, while **2** and **3** contain an aminobutyryl (C₄N) group that is further modified to a diazapenone ring.

The assembly of the ADR-GlyU disaccharide core has been previously delineated in vitro using the recombinant enzymes involved in **3** and **5** biosynthesis⁸⁻¹¹. The pathway requires six enzymes that convert UMP and L-Thr to the ADR-GlyU disaccharide (Supplementary Fig. 1a), and bioinformatic analysis suggests these steps are shared for **2** and **4** (the gene cluster for **1** is unknown)^{6,12}. However, the origin of the C₃N or C₄N units in these TL1 inhibitors and the mechanism for their incorporation onto the ADR-GlyU disaccharide scaffold has not been defined. Similar C₃N and C₄N units are found in several unrelated metabolites, for example various polyamines and siderophores, and they are known or hypothesized to be derived from either *S*-adenosyl-L-methionine (AdoMet) or, less frequently, L-Asp- β -semialdehyde¹³⁻¹⁵. Here we provide evidence to support a shared mechanism for the insertion of the C₃N group of **5** and the C₄N group of **3** that employs AdoMet as the direct metabolic precursor. Unlike other AdoMet-dependent alkylations, however, the process is highlighted by a fundamentally different catalytic strategy that involves γ -replacement by a pyridoxal-5'-phosphate (PLP)-dependent enzyme. Furthermore, the alkyl acceptor was unexpectedly determined to be the phosphorylated version of the ADR-GlyU disaccharide core, which was recently identified as the product of the kinase Mur28 from the **5** biosynthetic pathway¹⁶. Although not readily apparent from the structure, the same alkylation strategy is also shown to initiate the biosynthesis of the highly unusual dihydroxylated piperidine ring of **4**.

Results

Metabolic origin of C₃N and C₄N units

The metabolic origin of the alkylamine linker was initially examined using feeding experiments with isotopically labelled potential precursors. *Streptomyces* sp. NRRL 30475—a mutant strain of the native producer of muraymycins^{7,16}—was chosen as the model system due to the reproducible and relatively acceptable titers of **5** (Supplementary Note). Compound **5** contains a peptide that is predicted to be assembled by a nonribosomal peptide synthetase complex from L-Val, L-Arg, L-Leu and bicarbonate precursors (Supplementary Fig. 1b)¹⁷. Consequently, L-[1-¹³C]Leu was fed as a positive control, and **5** was isolated and confirmed by ¹H-NMR spectroscopy (Supplementary Fig. 2a). High resolution-mass spectrometry (HR-MS) revealed ~34% of **5** was enriched with a single ¹³C atom (Supplementary Fig. 3). Comparison of the ¹³C-NMR spectra revealed a clear enhancement of the 174.8 ppm signal that corresponds to the amide carbon of the Leu component, the expected site of incorporation (Supplementary Fig. 2b). HR-MS/MS was likewise consistent with the regioselective incorporation of L-[1-¹³C]Leu (Supplementary Fig. 4). Subsequently, L-[¹³C₅, ¹⁵N]Met, an established precursor of AdoMet, or L-[¹³C₄, ¹⁵N]Asp, an established precursor of L-aspartate β-semialdehyde, were individually fed to the strain, and the isolation of **5** was confirmed by ¹H-NMR spectroscopy (Supplementary Fig. 5). HR-MS analysis of **5** derived from the L-[¹³C₅, ¹⁵N]Met feeding experiments revealed ~31% consisting of a +5-amu isotopologue (Supplementary Fig. 6). Comparison of the ¹³C-NMR spectra suggested no substantial enrichment upon feeding L-[¹³C₄, ¹⁵N]Asp, while an increase in the signal intensity of four peaks was observed when feeding L-[¹³C₅, ¹⁵N]Met (Fig. 2). The peak signal at 58.0 ppm, previously assigned as the 2'' methyl ether, was enriched, which is consistent with alkylation catalyzed by an AdoMet-dependent O-methyltransferase. The remaining three signals at 45.6 (d), 25.0 (t), and 35.8 (dd) ppm—corresponding to C1'''-C3''' of the aminopropyl linker of **5**, respectively—were similarly enriched, which is consistent with AdoMet as the direct precursor. HR-MS/MS further supported these findings (Supplementary Fig. 7). The ¹J_{CC} splitting pattern and value (35.5 Hz) from L-[¹³C₅, ¹⁵N]Met feeding suggested an intact incorporation of the C₃N unit. Importantly, the peak corresponding to C3''' had a second coupling (7.8 Hz), which is consistent with expectations for ¹J_{CN} coupling in this chemical environment.

Aminobutyryltransferase functional assignment

C₃N and C₄N transferases with established functions have sequence and structural similarity to AdoMet-dependent methyltransferases^{13–15,18–20}. The gene cluster for **5** encodes for a single protein (Mur11) with an AdoMet-dependent MTase domain. Homologous genes, however, are not found in the **2–4** biosynthetic gene cluster, and the gene product was tentatively assigned as the catalyst for 2''-O-methylation to convert **6** to **5**. Armed with the knowledge that AdoMet or an L-Met-derived metabolite would ultimately need to undergo decarboxylation to generate **5**, similar to polyamine biosynthetic pathways that proceed through AdoMet decarboxylation prior to C₃N group transfer¹³, the gene cluster for **5** was further analyzed for the presence of any remaining gene encoding a putative PLP-dependent decarboxylase. This search uncovered Mur23, which has similarity to proteins annotated as diaminopimelate decarboxylases belonging to the conserved domain family of COG0019

(Supplementary Fig. 8). A Mur23 homolog is not encoded in the **2** and **3** gene cluster, as expected, if Mur23 is indeed a decarboxylase. Another putative PLP-dependent protein Mur24, with sequence similarity to proteins annotated as 1-aminocyclopropane-1-carboxylate (ACC) synthases, is encoded immediately downstream of *mur23*. The similarity of Mur24 to ACC synthases, which are PLP-dependent enzymes that utilize AdoMet to catalyze intramolecular C α -C γ bond formation with concomitant C γ -S bond cleavage to produce ACC and methylthioadenosine (MTA)²¹, was intriguing due to the evidence that L-Met—likely by way of AdoMet—serves as the C $_3$ N source of **5**. Phylogenetic analysis suggested that Mur24 occupies a separate clade, and hence might harbor a distinct activity, when compared to plant ACC synthases or the recently characterized bacterial ACC synthase, GnmY (Supplementary Fig. 9)²². In contrast to *mur23*, genes homologous to *mur24* were identified within the **2** (*cpz13*) and **3** (*lipJ*) gene clusters, suggesting that this enzymatic step is shared in these pathways^{12,23}. A gene (*sphL*) encoding a protein with sequence similarity to Mur24 was also identified within the **4** gene cluster⁶. The Mur24 homologs, which range from 34–50% in sequence identity using pairwise alignments, are part of the class I aminotransferase superfamily, and all retain a conserved Lys (corresponding to Lys234 for Mur24 and Lys229 for LipJ) that is predicted to be critical for PLP binding and enzymatic activity (Supplementary Fig. 10).

Recombinant Mur24, purified to near homogeneity from *Streptomyces lividans* TK24 (Supplementary Fig. 11), was initially screened for activity with two potential alkyl acceptors: (5', S, 6' S)-GlyU (**7**), the demonstrated isomeric product of LipK and Mur17 involved in **3** and **5** biosynthesis, respectively; and ADR-GlyU (**8**), the disaccharide product of the six-enzyme pathway that was previously characterized (Fig. 3a)^{9–11}. The acceptors were prepared by both chemical and chemoenzymatic synthesis, and the identity was confirmed by spectroscopic analyses (Supplementary Note). Based on the results from the isotopic enrichment experiments, L-Met, dcAdoMet, and AdoMet were tested as potential alkyl donors. Analysis of the reactions performed under a variety of conditions including with or without exogenously supplied PLP, however, failed to reveal a new peak. Reactions with recombinant LipJ and SphL (Supplementary Fig. 11) also gave negative results.

Mur28 was previously shown to catalyze the phosphorylation of the 3''-OH of **6** and **8**, the latter generating 3''-O-phospho-**8** (**9**) (Fig. 3a). Single-substrate kinetic analysis revealed an approximately 60-fold higher catalytic efficiency with **8**, suggesting that phosphorylation occurs prior to the attachment of the C $_3$ N-linked peptide component. Consequently, ATP and Mur28 were included in the Mur24 activity screen to generate **9** in situ as a potential alkyl acceptor for Mur24. HPLC analysis revealed the formation of a new peak that was dependent upon the inclusion of AdoMet (Fig. 3b). MS analysis was consistent with Mur24-catalyzed alkylation of **9** to generate **10** (Supplementary Note). Subsequently, **9** was enzymatically prepared and purified, and comparison of the MS and NMR spectra was consistent with 3''-OH as the site of phosphorylation as previously reported (Supplementary Note)¹⁶. Using purified **9** as the alkyl acceptor, the identical result was obtained (Fig 3c). HR-MS analysis of the product **10** yielded an (M + H)⁺ ion at $m/z = 630.1643$, which is consistent with the molecular formula for C $_4$ N-modified-**9** [expected (M + H)⁺ ion at $m/z = 630.1660$ for C $_{20}$ H $_{32}$ N $_5$ O $_{16}$ P]. Analysis by NMR spectroscopy (Supplementary Note)

further supported the structure of the Mur24 product **10** (Fig. 3a), and ^1H - ^{13}C HMBC correlations between C6' of GlyU and C1''' of the C₄N group supported the expected regiochemistry for C₄N attachment. The formation of **10** suggests 5'-deoxy-5'-(methylthio)adenosine (MTA) is generated as the co-product, which was detected by HR-MS (Supplementary Fig. 12). High background levels of MTA as a consequence of nonenzymatic AdoMet degradation, however, precluded a quantitative assessment (Fig. 3). Overall, the data are consistent with the functional assignment of Mur24 as an AdoMet:**9** aminobutyryltransferase (ABTase), generating **10** and likely MTA as co-products.

The activity of the Mur24 homologs LipJ and SphL, which are involved in the biosynthesis of **3** and **4**, respectively, was next interrogated. The gene cluster for **4** does not encode for a Mur28 phosphotransferase homolog, suggesting the possibility that phosphorylation of **8** is not a prerequisite for C₄N transfer by SphL. Conversely, the gene cluster for **3** encodes two Mur28 homologs, LipX (36% sequence identity) and LipI (23%), suggesting that LipJ has the same substrate specificity with respect to the alkyl acceptor as Mur24. Activity tests of LipJ with **9** and AdoMet revealed the formation of **10**, and the reaction was dependent upon a phosphorylated acceptor as the substrate (Supplementary Fig. 13a,b). Contrary to expectations, SphL catalyzed the same reaction wherein activity was strictly dependent upon a phosphorylated acceptor **9** as the substrate (Supplementary Fig. 13c), despite the absence of a phosphotransferase candidate. Overall the results establish the functional assignment of this group of proteins as AdoMet:**9** ABTases that catalyze γ -replacement of AdoMet, thereby breaking the C γ -S bond while generating a new C γ -N bond. Furthermore the results suggest that the biosynthesis of **3–5** occurs through **10**, an unexpected phosphorylated intermediate and the likely last shared intermediate of these pathways.

Biochemical characterization

Following the functional assignment of the newly discovered ABTases, the biochemical properties were examined primarily using Mur24 as the model enzyme. When PLP was omitted from the reaction, a trace amount of **10** was detected (Fig. 3c). Subsequently, a Mur24(K234A) mutant was prepared, and the activity was abolished with or without the addition of PLP (Supplementary Fig. 14). The same result was obtained with LipJ(K229A). Thus, the data are consistent with an important role for PLP in catalysis and that the Lys—predicted through bioinformatics analysis to form an internal aldimine with PLP—is essential (Supplementary Fig. 10). Potential alternative alkyl donor substrates that are known to be (or hypothetically could be) derived from L-Met—including (*S*)-methylmethionine (SMM), ACC, 2-amino-3-butenoic acid [commonly referred to as L-vinylglycine (L-VG)], L-homoserine lactone, and the AdoMet analogue sinefungin (Supplementary Fig. 15a)—were next tested with Mur24. Cystathionine and *O*-succinyl-L-homoserine were also screened as potential C₄N donors. Only SMM, an abundant plant metabolite that can be metabolized by some animals and bacteria²⁴, was able to substitute for AdoMet as an alkyl donor (Supplementary Fig. 15b). The relative activity with SMM was substantially reduced (9% yield of **10** relative to AdoMet), suggesting that AdoMet is the substrate in vivo. Using precolumn modification with 3-methyl-2-benzothiazolinone hydrazine hydrochloride (MBTH), a relatively minor amount of L-VG was converted to α -ketobutyrate (α KB) and NH₃ by Mur24. Time-course analysis gave a specific activity of 0.05 min⁻¹ for this reaction

(Supplementary Fig. 15c), a 54-fold reduction compared to the calculated turnover for the alkyl transfer reaction with AdoMet (vide infra). Thus, similarly to ACC synthase, L-VG serves as an alternative yet inferior substrate for an aminotransferase side reaction²¹. However, incubation of L-VG with Mur24 and **9** under a variety of reaction conditions did not yield detectable **10**. This result is in contrast to that observed with cystathionine γ -synthase (CSG synthase), which catalyzes γ -replacement of the α -amino acid *O*-succinyl-L-homoserine with the sulfhydryl group of L-Cys to generate L-cystathionine and succinate (Supplementary Fig. 16a) and is able to catalyze γ -addition starting with L-VG and L-Cys at pH 8.3 (ref. 25). Finally, the (*S*)- and (*R*)-sulfonium isomers of commercial AdoMet, the former being the biologically relevant diastereomer generated by AdoMet synthetase (MAT), were separated by HPLC and tested with Mur24 (Supplementary Fig. 17a). Unexpectedly, both isomers were functional as alkyl donors to convert **9** to **10** (Supplementary Fig. 17b).

The same panel of hypothetical alkyl donors was also tested for inhibition of the Mur24-catalyzed reaction using conditions promoting a near complete conversion of **9** to **10** with AdoMet as the alkyl group donor. SMM, which undergoes trace turnover when substituting for AdoMet under these conditions, inhibited the reaction at a 2:1 molar ratio relative to AdoMet (Supplementary Fig. 18a). Sinefungin, a well-known inhibitor of many AdoMet-dependent methyltransferases, likewise inhibited the Mur24-catalyzed formation of **10** using either AdoMet or SMM as the alkyl donor (Supplementary Fig. 18a). The remaining L-Met analogues including L-VG, which is an established mechanism-based inhibitor of ACC synthase^{26,27}, had no effect on **10** production (Supplementary Fig. 18b). Similarly, the addition of EDTA or Zn²⁺ or sulfhydryl-modifying reagents had no effect. Finally, by directly detecting the formation of **10** by HPLC, single-substrate kinetic analysis revealed Michaelis-Menten kinetics with respect to varied **9** (Supplementary Fig. 19), yielding a $K_m = 92 \pm 8 \mu\text{M}$ and $k_{cat} = 2.7 \pm 0.2 \text{ min}^{-1}$. The limiting amount of available **9** precluded an accurate assessment of the kinetic parameters for co-substrate AdoMet.

Mechanistic insight

Enzymatic alkyl group transfer from AdoMet to a nitrogen nucleophile of an acceptor substrate is generally considered to occur by S_N2 nucleophilic substitution. However, the PLP dependency of these newly discovered ABTases suggest γ -replacement with AdoMet occurs through a stepwise γ -elimination- γ -addition similar to CSG synthase^{25,28–30}. Mechanistic insight for PLP-dependent enzymes such as CSG synthase can often be garnered by monitoring PLP-bound intermediates by UV-Vis spectroscopy²⁸, however spectral snapshots of the Mur24 reaction under steady state conditions provided marginal information on the mechanism and role of PLP (Supplementary Fig. 20). We therefore opted to track the hydrogen atoms before and after C₄N group transfer as a way to discriminate between mechanistic possibilities. Three AdoMet isotopologues were prepared in situ using differentially deuterated L-Met and human MAT isoform 2A (hMAT2A) (Fig. 4). Starting with L-[2,3,3,4,4-²H₅; methyl-²H₃]Met and monitoring the Mur24-catalyzed formation of **10** by HR-MS, an (M + H)⁺ ion at $m/z = 633.1835$ was detected [expected (M + H)⁺ at $m/z = 633.1848$ for C₂₀H₂₉D₃N₅O₁₆P], consistent with the retention of 3 of 8 deuterium atoms when compared to unlabeled L-Met control (detected $m/z = 630.1615$). An (M + H)⁺ ion at $m/z = 633.1859$ was observed with L-[2,3,3,4,4-²H₅]Met, again indicating the retention of 3

deuterium atoms. Finally, an $(M + H)^+$ ion at $m/z = 630.1653$ was detected when starting with L-[2- ^2H]Met, revealing the loss of the single deuterium during the formation of **10**.

Reactions starting with **9** and natural abundance AdoMet were performed in D_2O , and isotopic distribution revealed that most of **10** was monodeuterated (60%) with some dideuterated (19%) after 6 h (Supplementary Fig. 21a). The potential reversibility of the Mur24-catalyzed reaction was also examined. Although no products were observed when starting with **10** and MTA, time-course analysis of reactions in D_2O revealed a relatively fast incorporation of one deuterium into **10** (specific activity of $1.2 \mu\text{mol}/\text{min}/\text{mg} \approx 62 \text{ min}^{-1}$) and a slow formation of dideuterated-**10** ($2.0 \times 10^{-2} \mu\text{mol}/\text{min}/\text{mg} \approx 1.0 \text{ min}^{-1}$) (Supplementary Fig. 21b,c). After a 6-h reaction, isotopic distribution revealed that most of **10** was monodeuterated (75%) with some dideuterated (9%). Overall, the data are consistent with two exchangeable hydrogen atoms from AdoMet—one bonded to C-2 and the other C-3 or C-4—during the C_4N group transfer reaction.

Enzymatic decarboxylation of **10**

The functional assignment of the PLP-dependent ABTases suggested that, unlike classical AdoMet-dependent polyamine biosynthesis, decarboxylation during **5** biosynthesis occurs after alkyl group transfer. To explore this possibility, recombinant Mur23 was produced and purified (Supplementary Fig. 11d). Unlike the ABTases, Mur23 copurified with PLP as evident by the yellow color and the characteristic UV/Vis spectrum (Supplementary Fig. 22). LC-MS analysis of reactions of Mur23 with **10** yielded a new peak (Fig. 5) with an $(M + H)^+$ ion at $m/z = 586.1748$, consistent with the molecular formula for decarboxylated-**10** (**11**) [expected $(M + H)^+$ 586.1756 for $\text{C}_{19}\text{H}_{32}\text{N}_5\text{O}_{14}\text{P}$] (Supplementary Note). The structure of **11** was further supported by MS and NMR spectroscopy (Supplementary Note). In contrast to reactions with **10**, Mur23 was unable to catalyze decarboxylation of AdoMet or dephospho-**10** (**12**) (Supplementary Fig. 23), the latter generated by reacting **10** with calf intestinal phosphatase and confirmed by MS (Supplementary Note). Single-substrate kinetic analysis revealed Michaelis-Menten kinetics with respect to varied **10** (Supplementary Fig. 19b), yielding a $K_m = 701.8 \pm 9.2 \mu\text{M}$ and $k_{cat} = 144.8 \pm 1.1 \text{ min}^{-1}$, equating to an apparent second order rate constant $k_{cat}/K_m \sim 3.3 \times 10^3 \text{ M}^{-1}\text{s}^{-1}$, a 6-fold greater catalytic efficiency compared to Mur24 ($k_{cat}/K_m \sim 5 \times 10^2 \text{ M}^{-1}\text{s}^{-1}$). The K_m value for Mur23, although relatively high, is within the range observed for other PLP-dependent decarboxylases (Supplementary Fig. 8). Overall the data support the functional assignment of Mur23 as a **10** decarboxylase (Fig. 5b).

Discussion

AdoMet is perhaps best known as a methyl donor, although this ubiquitous metabolite also serves as the source for C_3N and C_4N alkyl groups in the biosynthesis of many structurally distinct metabolites. For C_3N group biosynthesis, a PLP-dependent decarboxylase first generates dcAdoMet, which serves as the substrate for a distinct alkyltransferase that catalyzes C_3N group transfer independent of cofactors. These C_3N alkyltransferases have structural similarity to AdoMet-dependent methyltransferases and consequently have been proposed to originate via divergent evolution. AdoMet as a C_4N group donor has likewise

been noted in several metabolic pathways^{14,20,31–34}. Similarly to the C₃N alkyltransferases, the available data suggest the C₄N alkyltransferases are also structurally, mechanistically, and evolutionarily related to methyltransferases^{18,19}. The data herein have provided evidence of a C₄N alkyl group transfer from AdoMet by a new family of enzymes most closely related to plant PLP-dependent ACC synthases^{26,35}.

Canonical AdoMet- or dcAdoMet-dependent alkyl group transfer is generally believed to occur by an S_N2 substitution, wherein the nucleophile directly attacks the carbon adjacent to the sulfonium. Consequently, no exchange of carbon-bonded hydrogen atoms would be expected during the reaction. Similarly, the ACC synthase reaction proceeds without exchange²¹. The results with Mur24 revealed two exchangeable hydrogen atoms, which is consistent with alkyl group transfer from AdoMet via a stepwise reaction proceeding through sequential γ -elimination (lyase) and aza-Michael γ -addition (synthase) chemistries. Although less-favored mechanisms remain possible, we propose the following mechanism that is comparable to the γ -replacement mechanism put forth for CSG synthase (Fig. 6)^{28–30,36}. PLP and AdoMet first generate an external aldimine I that is commonplace for PLP-dependent enzymes. Interestingly, unlike many PLP-dependent enzymes including CSG synthase²⁸, the recombinant ABTases do not co-purify with PLP under a variety of conditions screened. Following the formation of a pseudo-Michaelis (ternary) complex, a general base—likely Lys234 for Mur24—abstracts the C _{α} proton. This step, again well established for many PLP-dependent enzymes, is supported by the deuterium labelling experiments. Due to the lack of a diagnostic absorption band for a quinonoid (Supplementary Fig. 20), C _{α} deprotonation is likely immediately followed by C4' protonation, generating the ketimine II. Subsequently, the C _{β} proton—rendered relatively more acidic due to the vicinal iminium—is abstracted to form the enamine III prior to formation of a transient β,γ -unsaturated ketimine IV with concomitant elimination of MTA. The intermediacy of enamine III is supported by the deuterium “wash-in” experiments with **10**, which demonstrate Mur24-catalyzed exchange of the α and β hydrogens without γ -elimination. In the presence of **9**, i.e. the true Michaelis complex, the amine nucleophile is deprotonated by an unidentified general base and attacks C _{γ} in an aza-Michael-type nucleophilic addition, and the reverse of the previous steps affords **10**.

Potentially the most intriguing feature of the Mur24-catalyzed reaction is the chemical functionality involved in the bond-breaking and bond-making steps to transform one γ -substituted, α -amino acid to another. CSG synthase and *O*-acetyl-L-homoserine sulfhydrylase³⁷, enzymes catalyzing a native PLP-dependent γ -replacement, initiate their reactions by breaking a C _{γ} -OC(O)R bond prior to the formation of a new C _{γ} -S bond (Supplementary Fig. 16a). These enzymes along with two other PLP-dependent enzymes, L-Met γ -lyase and cystathionine γ -lyase, have been shown to catalyze reactions in vitro using nucleophiles other than thiols including selenium/selenols (C _{γ} -Se), and cyanide (C _{γ} -C), although the biological relevance of these reactions is unknown (Supplementary Fig. 16b)^{38–41}. Mur24 and homologous ABTases are clearly different than these γ -replacement enzymes by utilizing a sulfonium substrate, thereby breaking a C _{γ} -S⁺ bond, and using a primary amine of an amino acid acceptor, thereby generating a C _{γ} -N bond. This aza-Michael-type 1,4-addition, a comparable second half-reaction of which has been proposed

during ergot alkaloid biosynthesis but for which the putative enzyme catalyst has not yet been characterized (Supplementary Fig. 16c)⁴², is a considerable chemical feat. The general interest in having mild and simple methodologies to introduce unfunctionalized C-N bonds via aza-Michael additions has resulted in multiple reports detailing new synthetic catalysts and strategies^{43,44}. Consequently, a few enzymes have been discovered to catalyze an aza-Michael-type γ -addition that is similar to the addition half-reaction addressed here, although an entirely different, PLP-independent catalytic strategy is used to afford a new C-N bond^{45,46}. Interestingly, an enzyme SbnA involved in the biosynthesis of L-2,3-diaminopropionic acid has recently been shown to catalyze a PLP-dependent β -replacement reaction utilizing the amine of L-Glu as a nucleophile for addition⁴⁷. However, the reaction involves a β -replacement as opposed to the γ -replacement, a fundamental difference between the two enzymes. The catalytic strategy used by Mur24 and SbnA to activate amine nucleophiles for γ - and β -addition reactions, respectively, and how this compares with other β - and γ -replacement enzyme catalysts, can now be addressed.

CSG synthase catalyzes a well-characterized γ -replacement reaction with a specific activity of 100 $\mu\text{mol}/\text{min}/\text{mg}$ ($\sim 240 \text{ min}^{-1}$)³⁰. CSG synthase is also able to convert L-VG and L-Cys to cystathionine, thereby bypassing the first-half (i.e., γ -elimination) reaction²⁵. The newly discovered ABTases cannot bypass the elimination step by using L-VG as an alkyl donor. The ability of CSG synthase to use L-VG directly for γ -addition has been speculated to be a consequence of solvent accessibility to the active site²⁵, which compensates for the incorrect protonation state of the general base/acid (EnzB₁ in Fig. 6) responsible for C _{β} deprotonation (during γ -elimination) and re-protonation (during γ -addition). Using cystathionine, CSG synthase catalyzes isotope exchange from ³H₂O to both C _{α} and C _{β} protons—with a 2-fold preference for C _{β} exchange over C _{α} —at rates >7-fold faster than the overall γ -replacement reaction³⁰. Mur24 can catalyze a similar isotope exchange from D₂O to **9** that is comparably faster (~ 23 -fold) than γ -replacement. However, the data establish a strong preference for the exchange of a single hydrogen per molecule instead of two (62-fold difference), suggesting that one site, which we propose is C _{β} , is better shielded from bulk solvent and hence cannot support γ -addition starting with L-VG. The differences in reactivity of CSG synthase and the ABTases could also be the result of the nature of the acceptor nucleophile. Thiols/thiolates, for example, the L-Cys acceptor for CSG synthase, are excellent nucleophiles for conjugate additions, and the softness enables orbital effects to dominate the reaction with the relatively soft electrophilic center at C _{γ} ^{48,49}. The PLP-dependent ABTases utilize a relatively hard amine nucleophile, thereby relying more on charges and electrostatic effects to catalyze conjugate γ -addition. Consequently, the correct protonation state is likely critical for PLP-dependent ABTase activity, and this can only be achieved upon catalyzing γ -elimination of the substrate. Ongoing structural and biochemical studies will undoubtedly help clarify the observed differences in the chemistry.

Finally, the discovery of the PLP-dependent C₄N alkyltransferases has revealed that the biosynthetic pathway for **3–5** proceeds through a cryptic phosphorylated intermediate. This discovery is consistent with the isolation of a phosphorylated caprazol from a mutant strain of the **2** producer⁵⁰, as well as the previous functional assignment of the kinase Mur28 involved in **5** biosynthesis¹⁶. The results establish **10** as the most likely last shared

intermediate, upon which the pathways diverge to afford the structurally unique scaffolds of **1–5**. Pathway divergence for **5** is initiated by Mur23-catalyzed **10** decarboxylation that, when combined with the preceding Mur24-catalyzed alkyl transfer, has revealed a new, “inverse” polyamine biosynthetic strategy using two consecutive PLP-dependent enzymes to incorporate an aminopropyl linker derived from the exceptionally versatile metabolite AdoMet.

Statistics and Reproducibility

HPLC traces and MS spectra are representative of data collected minimally twice independently with similar results. Data points in scatter plots represent the average of three independent experiments unless noted in the figure legend, and the error bars depict the standard deviation.

Methods

Chemicals, Bacterial Strains and Instrumentation

Chemicals and solvents were purchased from standard sources. L-[2,3,3,4,4-²H₅; methyl-²H₃]Met, L-[2,3,3,4,4-²H₅]Met and L-[2-²H]Met were purchased from CDN isotopes. An (*S*)- and (*R*)-AdoMet mixture (~3:2) was purchased from Santa Cruz Biotechnology (Dallas, TX). Compounds **7** and **8** were prepared as described (Supplementary Note)^{16,51,52}. Synthetic oligonucleotides were purchased from Integrated DNA Technologies (Coralville, IA). Phusion DNA polymerase, restriction enzymes and T4 DNA ligase were obtained from New England Biolabs Inc (Ipswich, MA) and used according to the manufacturer’s instructions. LA-Taq polymerase was obtained from Takara Bio Inc. (Shiga, Japan). DNA sequencing was carried out by ACGT Inc (Wheeling, IL). Muraymycin-producing strains *Streptomyces* sp. NRRL30475 and NRRL30473 were obtained from the ARS Culture Collection (NRRL). *E. coli* NEB5 α , *E. coli* BL21(DE3), and *Streptomyces lividans* TK24 were used for routine cloning and protein expression.

NMR data was recorded at 400 MHz for ¹H and 100 MHz for ¹³C with a Varian Inova NMR spectrometer or 600 MHz for ¹H and 150 MHz for ¹³C with Agilent 600/54 NMR spectrometer. HPLC analysis was performed on an Agilent 1200 system equipped with a photodiode array detector and an analytical SeQuant[®] ZIC[®]-HILIC column (5 μ m, 200 Å , 250 \times 4.6 mm), an Alltech[®] Apollo[™] C18 column (5 μ m, 100 Å , 250 \times 4.6 mm), or a Thermo Scientific[™] Acclaim[™] 120 C18 column (5 μ m, 120 Å , 100 \times 4.6 mm). Semi-preparative HPLC was performed on a Waters 600 equipped with a photodiode array detector and an Alltech[®] Apollo[™] C18 column (5 μ m, 100 Å , 250 \times 10 mm). LC-MS was conducted with an Agilent 6120 Quadrupole MSD mass spectrometer equipped with an Agilent 1200 Series Quaternary LC system. HR-ESI-MS spectra were acquired with an AB SCIEX Triple TOF 5600 System or Agilent 6230 TOF LC/MS System.

Isotopic Enrichment

Growth conditions for *Streptomyces* sp. NRRL30475 were as previously described (Supplementary Note)¹⁶. A seed culture was incubated at 30 $^{\circ}$ C for 72 h, when 2 mL was used to inoculate 50 mL of fresh medium. After fermentation for 65 h, 25 mg of filter-

sterilized L-[1-¹³C]Leu, L- [¹³C5, ¹⁵N]Met or L-[¹³C4, ¹⁵N]Asp was added to each 250-mL flask containing 50 mL of medium. Fermentation was continued an additional 72 h. Compound **5** was extracted and purified as previously described (Supplementary Note). Percent enrichment was calculated based on the theoretical and observed isotopic distribution of **5**.

Cloning for gene expression

Genes were cloned from genomic DNA using standard procedures (primers listed in Supplementary Table 1). The gel-purified PCR product for *mur24* or *mur23* was digested with *NdeI*-*Bam*HI and ligated to the identical sites of pXY200 to yield pXY200-*mur24* and pXY200-*mur23*, respectively. PCR integrity was confirmed by DNA sequencing. The gel-purified PCR product for *lipJ* was sequenced and inserted into pET30Xa/LIC vector using ligation-independent cloning following the provided protocol. The gene *sphL* was synthesized by Genscript and subcloned into pET30Xa/LIC vector for expression.

Site-directed mutagenesis

A K234A point mutation of Mur24 and a K229A point mutation of LipJ were generated by PCR amplification with Q5 hot start high-fidelity DNA polymerase using pET30-*mur24* or pET30-*lipJ* as a template, respectively. The template pET30-*mur24* was obtained using ligation-independent cloning with pET30 Xa/LIC vector following the provided protocol. PCR product was digested with 10 units of *DpnI* for 2 h at 37 °C and transformed into *E. coli* NEB5 α competent cells. The sequence of the entire gene with the introduction of the correct point mutation was confirmed by sequencing. Plasmid pET30-*mur24*(K234A) was digested with *NdeI*-*Bam*HI, and the DNA fragment of the expected size was purified and ligated to the identical sites of pXY200 to yield pXY200-*mur24*(K234A).

Recombinant protein production

Plasmids pXY200-*mur24*, pXY200-*mur24*(K234A), and pXY200-*mur23* were transformed into *S. lividans* TK24 using PEG-mediated protoplast transformation and plated on R2YE supplemented with 50 μ g/mL apramycin. After 6 days at 28 °C, positive transformants were confirmed by colony PCR using InstaGene Matrix from Bio-Rad and LA-Taq polymerase with GC buffer I. Positive strains were utilized to inoculate 50 mL of R2YE containing 50 μ g/mL apramycin, grown for 3 days at 28 °C at 250 rpm, and 2 mL transferred to 100 mL of fresh R2YE containing 50 μ g/mL apramycin. Following growth for 3 days at 28 °C at 250 rpm, protein expression was induced by the addition of thiostrepton (5 μ g/mL) and the culture was incubated for another 24 h before harvesting. The cells from 400 mL of culture were collected by centrifugation. The pellet was thoroughly resuspended in ice-cold Buffer A (100 mM KH₂PO₄, 300 mM NaCl, 10 mM imidazole, pH 8.3) supplemented with 4 mg/mL of lysozyme was subsequently added to the suspension. After incubation at 30 °C for 30 min, the cell suspension was mixed by pipetting and lysed using a Qsonica sonicator for a total of 8 min at 40% amplitude with 10 s pulses separated by 50 s rest periods. Following centrifugation, the protein was purified using affinity chromatography with HisPur™ Ni-NTA agarose, and proteins were eluted with increasing concentrations of imidazole in Buffer A. Purified proteins were concentrated and buffer exchanged into Buffer B (25 mM

KH₂PO₄, 100 mM NaCl, pH 8.3) using Amicon[®] Ultra 10000 MWCO centrifugal filters and stored as glycerol stocks (40%) at -20 °C. Protein purity was assessed as by 12% acrylamide SDS-PAGE; His₆-tagged proteins were utilized without further modifications.

Plasmids pET30-*lipJ*, pET30-*lipJ*(K229A), and pET28a-*sphL* were introduced into BL21(DE3), and the transformed strains were grown in LB supplemented with 50 µg/mL kanamycin or ampicillin. Following inoculation of 500 mL of LB with 50 µg/mL kanamycin or ampicillin, the cultures were grown at 37 °C until the cell density reached an OD₆₀₀ ~ 0.5 when expression was induced with 0.1 mM IPTG. Cells were harvested and processed as described above.

Reactions with Mur28 and Mur24

Reactions consisted of 25 mM potassium phosphate (pH 8.3), 500 µM **8**, 500 µM AdoMet, 1 mM ATP, 1 mM MgCl₂, 100 µM PLP, and 200 nM Mur28 and Mur24 for 3 h at 30 °C, and the reaction was subsequently quenched by adding two volumes of acetonitrile followed by centrifugation (21000 × g, 30 min) to remove the precipitated protein. The reaction was monitored by LC-MS or HPLC using a SeQuant[®] ZIC[®]-HILIC column (5 µm, 200 Å, 250 × 4.6 mm). A series of linear gradients was developed from 0.1% formic acid (A) to acetonitrile with 0.1% formic acid (B) in the following manner (beginning time and ending time with linear change to % B): 0–12 min, 80% B; 13–26 min, 50% B; 27–35 min, 80% B; 35–50 min, 80%B. The flow rate was kept constant at 0.4 mL/min, and elution was monitored at 260 nm. Pre-column derivatization with AQC, a derivatizing reagent for amines⁵³, was also used to detect **10**. The reaction (20 µL) was mixed with 60 µL of 0.2 M sodium borate buffer (pH = 8.8) and 20 µL of 3 mg/mL AQC-acetonitrile solution. The mixtures were incubated at 55 °C for 10 min and then allowed to cool to room temperature. The AQC-derivatized samples (50 µL) were analyzed by LC-MS using an Alltech[®] Apollo[™] C18 column (5 µm, 100 Å, 250×4.6 mm) with detection at 260 nm using mobile phase A (0.1% formic acid) and B (acetonitrile with 0.1% formic acid). A gradient was applied as follows: linear gradient from 1% to 20% B for 10 min, then to 60% B over 15 min, followed by a hold of 100% B for 5 min, then to 1% B for 5 min at a flow rate of 0.4 mL/min.

Reactions with Mur24 or LipJ

Reactions consisted of 25 mM potassium phosphate (pH 8.3), 500 µM **9**, 500 µM potential aminopropyl donor (AdoMet, SMM, L -VG or ACC), 100 µM PLP and 200 nM enzyme [Mur24, Mur24 (K234A), LipJ, LipJ (K229A) or SphL for 6 h at 30 °C. The reaction was terminated by adding two volumes of cold acetonitrile followed by centrifugation (21000 × g, 30 min) to remove the precipitated protein. The reaction was monitored by LC-MS or HPLC using a SeQuant[®] ZIC[®]-HILIC column as described above.

Purification of AdoMet isomers

(*S*)- and (*R*)-forms of AdoMet was purified by HPLC⁵⁴ with a C18 reversed phase analytical column (Kinetex[™] 5 µm, 100 Å, 250×4.6 mm from Phenomenex) using 50 mM ammonium acetate buffer (pH=5.4) with 1% TFA.

Detection of α -ketobutyrate

Reactions consisted of 50 mM potassium phosphate (pH 8.3), 500 μ M AdoMet, 100 μ M PLP and 400 nM enzyme for 6 h at 30 °C, and the reaction was terminated by ultrafiltration using Amicon® Ultra 3000 MWCO centrifugal filters. Samples were treated with MBTH as previously described⁵⁵. In short, reaction mixtures (50 μ L) were mixed with 50 μ L of 1 M sodium acetate (pH 5.0) and 50 μ L of 8 mM MBTH aqueous solution. The mixtures were then incubated at 50 °C for 30 min and analyzed by using LC-MS with an analytical Thermo Scientific™ Acclaim™ 120 C18 column (5 μ m, 120 Å, 100 \times 4.6 mm) using mobile phase A and B. A gradient was applied as follows: linear gradient from 10% to 40% B for 15 min, 40% to 100% B for 10 min followed by a hold of 100% B for 7 min, then to 10% D for 2 min at a flow rate of 0.4 mL/min. Elution was monitored at 325 nm.

UV-Vis spectral analysis

Absorbance spectra were recorded on a BioTek™ Synergy™ 2 Multi-Mode Microplate Reader using 30 μ M indicated protein with 1 mM respective substrates at 30 °C in Buffer B supplemented with 100 μ M PLP, 1 mM AdoMet, 500 μ M compound **9** or 500 μ M compound **10**. Spectra were recorded every 1 min.

Activity of Mur24 with potential inhibitors

Reactions consisted of 25 mM potassium phosphate (pH 8.3), 250 μ M **9**, 0.5 mM AdoMet, 100 μ M PLP, potential inhibitors (2 mM L-VG, 1 mM sinefungin or 0.5 mM SMM) and 200 nM Mur24 for 3 h at 30 °C. The reactions were terminated by adding two volumes of cold acetonitrile followed by centrifugation. The reaction was monitored by LC-MS or HPLC using a SeQuant® ZIC®-HILIC column as described above.

Reactions with hMAT2A and Mur24

The reaction consisted of 50 mM potassium phosphate (pH 8.5), 50 mM KCl, 10 mM MgCl₂, 8 mM ATP, 1 mM L-Met, 40 μ M PLP, 250 μ M **9**, and 10 μ M hMAT2A and 200 nM Mur24 for 3–6 h at 30 °C, and the reaction was subsequently quenched by adding two volumes of acetonitrile followed by centrifugation (21000 \times g, 30 min) to remove the precipitated protein. The reaction components were analyzed by LC-MS using a SeQuant® ZIC®-HILIC column as described above.

Reaction with Mur24 in D₂O

The reaction (25 μ L) consisted of 50 mM potassium phosphate (pH 8.5), 50 mM KCl, 10 mM MgCl₂, 8 mM ATP, 1 mM L-Met, 40 μ M PLP, 250 μ M **9**, 10 μ M hMAT2A and 200 nM Mur24 for 6 h in D₂O (D₂O final percentage 80%) at 30 °C. Identical reactions were performed by starting directly with commercial AdoMet and consisted of 50 mM potassium phosphate (pH 8.5), 500 μ M **9**, 1 mM AdoMet, 40 μ M PLP and 200 nM enzyme Mur24 in D₂O (D₂O final percentage 80%) for 6 h at 30 °C. The reaction was also performed by starting with Mur24-product **10** and consisted of 50 mM potassium phosphate (pH 8.5), 500 μ M **10**, 100 μ M PLP and 200 nM enzyme Mur24 in D₂O (D₂O final percentage 80%) for the indicated time points at 30 °C. All reactions were quenched by adding two volumes of

acetonitrile followed by centrifugation. The supernatant was dried, reconstituted in H₂O, and incubated for 10 min prior to HR-ESI-MS analysis.

Activity of Mur23

Reactions consisted of 25 mM potassium phosphate (pH 8.3), 500 μM **10**, 100 μM PLP and 200 nM Mur23 for 1 h at 30 °C, and the reaction was terminated by adding two volumes of cold acetonitrile followed by centrifugation. For reactions containing calf intestinal phosphatase, reactions consisted of Cutsmart buffer, 25 mM potassium phosphate (pH 8.3), 500 μM **10**, 100 μM PLP, with or without 500 units/mL CIP for 30 mins at 37 °C. The reaction components were analyzed by LC-MS using a SeQuant[®] ZIC[®]-HILIC column as described above.

Kinetics of Mur23 and Mur24

Reactions consisted of 25 mM potassium phosphate (pH 8.3), 100 μM PLP, near saturating AdoMet (2 mM) with variable **9** (5 μM–500 μM). The reaction was performed at 30 °C with 200 nM Mur24 for 180 min and analyzed under initial velocity conditions. For Mur23 reactions consisted of 25 mM potassium phosphate (pH 8.3), 100 μM PLP with variable **10** (5 μM–1000 μM). The Mur23-catalyzed reaction was performed at 30 °C with 50 nM Mur23 for 60 min and analyzed under initial velocity conditions (<10% conversion). Product formation was determined using HPLC with the gradient described above. Each data point represents a minimum of three replicate end point assays; kinetic constants were obtained by nonlinear regression analysis using GraphPad Prism (GraphPad Software, La Jolla, CA).

Reporting Summary

Additional information on the research design is available in the Nature Research Reporting Summary linked to this article.

Data availability

All plasmids and raw data are available upon request. Sequences are deposited at NCBI under accession no. Mur24, ADZ45336; Mur23, ADZ45335; LipJ, BAJ05886; and SphL, BAO20191.

Supplementary Material

Refer to Web version on PubMed Central for supplementary material.

Acknowledgements

This work was supported in part by the National Institutes of Health Grants AI087849 and GM115261, the National Center for Advancing Translational Sciences Grant UL1TR000117, the Deutsche Forschungsgemeinschaft (DFG, grant DU 1095/5-1), the state of Lower Saxony [Lichtenberg doctoral fellowship (CaSuS program) for A.L.], the Konrad-Adenauer-Stiftung (doctoral fellowship for D.W.), and the Fonds der Chemischen Industrie (doctoral fellowship for G.N.). NMR (600 MHz) data was collected at the NMR facility of the Center for Environmental Systems Biochemistry supported in part by NIH grant DK097215. We would also like to acknowledge the Department of Pharmaceutical Sciences and the College of Pharmacy for financial support for MS and NMR instrumentation.

References

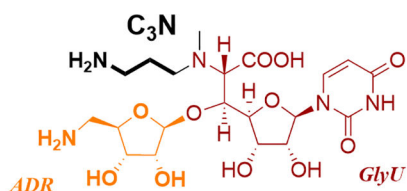
1. Winn M, Goss RJ, Kimura K, & Bugg TD Antimicrobial nucleoside antibiotics targeting cell wall assembly: recent advances in structure-function studies and nucleoside biosynthesis. *Nat. Prod. Rep* 27, 279–304 (2010). [PubMed: 20111805]
2. Shiraishi T & Kuzuyama T Recent advances in the biosynthesis of nucleoside antibiotics. *J. Antibiot* 72, 913–923 (2019). [PubMed: 31554958]
3. Hirano S, Ichikawa S, & Matsuda A Total synthesis of (+)-FR-900493 and establishment of its absolute stereochemistry. *Tetrahedron*, 63, 2798–2804 (2007).
4. Igarashi M, Takahashi Y, Shitara T, Nakamura H, Naganawa H, Miyake T, & Akamatsu Y Caprazamycins, novel lipo-nucleoside antibiotics, from *Streptomyces* sp. II. Structure elucidation of caprazamycins, *J. Antibiot* 58, 327–337 (2005). [PubMed: 16060385]
5. Fujita Y, Kizuka M, Funabashi M, Ogawa Y, Ishikawa T, Nonaka K, & Takatsu T A-90289 A and B, new inhibitors of bacterial translocase I, produced by *Streptomyces* sp. SANK 60405. *J. Antibiot* 64, 495–501 (2011). [PubMed: 21587261]
6. Funabashi M, Baba S, Takatsu T, Kizuka M, Ohata Y, Tanaka M, Nonaka K, Spork AP, Ducho C, Chen WC, & Van Lanen SG Structure-based gene targeting discovery of sphaerimicin, a bacterial translocase I inhibitor. *Angew. Chem. Int. Ed* 52, 11607–11611 (2013).
7. McDonald LA, Barbieri LR, Carter GT, Lenoy E, Lotvin J, Peterson PJ, Siegel MM, Singh G, & Williamson RT Structures of the muraymycins, novel peptidoglycan biosynthesis inhibitors. *J. Am. Chem. Soc* 124, 10260–10261 (2002). [PubMed: 12197711]
8. Yang Z, Chi X, Funabashi M, Baba S, Nonaka K, Pahari P, Unrine J, Jacobsen JM, Elliott GI, Rohr J, & Van Lanen SG Characterization of LipL as a non-heme, Fe(II)-dependent α -ketoglutarate:UMP dioxygenase that generates uridine-5'-aldehyde during A-90289 biosynthesis. *J. Biol. Chem* 286, 7885–7892 (2011). [PubMed: 21216959]
9. Barnard-Britson S, Chi X, Nonaka K, Spork AP, Tibrewal N, Goswami A, Pahari P, Ducho C, Rohr J, & Van Lanen SG Amalgamation of nucleosides and amino acids in antibiotic biosynthesis: discovery of an L-threonine:uridine-5'-aldehyde transaldolase. *J. Am. Chem. Soc* 134, 18514–18517 (2012). [PubMed: 23110675]
10. Chi X, Pahari P, Nonaka K, & Van Lanen SG Biosynthetic origin and mechanism of formation of the aminoribosyl moiety of peptidyl nucleoside antibiotics. *J. Am. Chem. Soc* 133, 14452–14459 (2011). [PubMed: 21819104]
11. Cui Z, Liu X, Overbay J, Cai W, Wang X, Lemke A, Wiegmann D, Niro G, Thorson JS, Ducho C, & Van Lanen SG Enzymatic synthesis of the ribosylated glycyL-uridine disaccharide core of peptidyl nucleoside antibiotics. *J. Org. Chem* 83, 7239–7249 (2018). [PubMed: 29768920]
12. Kaysser L, Lutsch L, Siebenberg S, Wemakor E, Kammerer B, & Gust B Identification and manipulation of the caprazamycin gene cluster lead to new simplified liponucleoside antibiotics and give insights into the biosynthetic pathway. *J. Biol. Chem* 284, 14987–14996 (2009). [PubMed: 19351877]
13. Michael AJ Biosynthesis of polyamines and polyamine-containing molecules. *Biochem. J* 473, 2315–2329 (2016). [PubMed: 27470594]
14. Dreyfus C, Lemaire D, Mari S, Pignol D, & Arnoux P Crystallographic snapshots of iterative substrate translocations during nicotianamine synthesis in archaea. *Proc. Natl. Acad. Sci. USA*, 106, 16180–16184 (2009). [PubMed: 19805277]
15. Lee J, Sperandio V, Frantz DE, Longgood J, Camilli A, Phillips MA, & Michael AJ An alternative polyamine biosynthetic pathway is widespread in bacteria and essential for biofilm formation in *Vibrio cholera*. *J. Biol. Chem* 284, 9899–9907 (2009). [PubMed: 19196710]
16. Cui Z, Wang X, Liu X, Lemke A, Koppermann S, Ducho C, Rohr J, Thorson JS, & Van Lanen SG Self-resistance during muraymycin biosynthesis: a complementary nucleotidyltransferase and phosphotransferase with identical modification sites and distinct temporal order. *Antimicrob. Agents Chemother* 62, e00193–18 (2018). [PubMed: 29735559]
17. Cheng L, Chen W, Zhai L, Xu D, Huang T, Lin S, & Deng Z Identification of the gene cluster involved in muraymycin biosynthesis from *Streptomyces* sp. NRRL 30471. *Mol. Biosyst* 7, 920–927 (2011). [PubMed: 21180767]

18. Ikeguchi Y, Bewley MC, & Pegg AE Aminopropyltransferases: function, structure, and genetics. *J. Biochem* 139, 1–9 (2006). [PubMed: 16428313]
19. Martin JL & McMillan FM SAM (dependent) I AM: The S-adenosylmethioine-dependent methyltransferase fold. *Curr. Opin. Struct. Biol* 12, 783–793 (2002). [PubMed: 12504684]
20. Reeve AM, Breazeale SD, & Townsend CA Purification, characterization, and cloning of an S-adenosylmethionine-dependent 3-amino-3-carboxypropyltransferase in nocardicin biosynthesis. *J. Biol. Chem* 1998, 30695–30703 (1998).
21. Ramalingam K, Lee K-M, Woodard RW, Bleecker AB, & Kende H Stereochemical course of the reaction catalyzed by the pyridoxal phosphate-dependent enzyme 1-aminocyclopropane-1-carboxylate synthase. *Proc. Natl. Acad. Sci. USA* 82, 7820–7824 (1985). [PubMed: 3865199]
22. Xu Z, Pan G, Zhou H & Shen B Discovery and characterization of 1-aminocyclopropane-1-carboxylic acid synthase of bacterial origin. *J. Am. Chem. Soc* 149, 16957–16961 (2018).
23. Funabashi M, Baba S, Nonaka K, Hosobuchi M, Fujita Y, Shibata T, & Van Lanen SG The biosynthesis of liposidomycin-like A-90289 antibiotics featuring a new type of sulfotransferase. *ChemBioChem* 11, 184–190 (2010). [PubMed: 20043306]
24. Ko S, Eliot AC, & Kirsch JF S-methylmethionine is both a substrate and an activator of 1-aminocyclopropane-1-carboxylate synthase. *Arch. Biochem. Biophys* 42, 85–90 (2004).
25. Johnston M, Marcotte P, Donovan J & Walsh C Mechanistic studies with vinylglycine and β -haoloaminobutyrate as substrates for cystathionine γ -synthase from *Salmonella typhimurium*. *Biochemistry*, 18, 1729–1738 (1979). [PubMed: 373802]
26. Feng L & Kirsch JF L-Vinylglycine is an alternative substrate as well as mechanism-based inhibitor of 1-aminocyclopropane-1-carboxylate synthase. *Biochemistry*, 39, 2436–2444 (2000). [PubMed: 10704193]
27. Capitani G, Tschopp M, Eliot AC, Kirsch JF, & Grütter MG Structure of ACC synthase inactivated by the mechanism-based inhibitor L-vinylglycine. *FEBS Lett* 579, 2458–2462 (2005). [PubMed: 15848188]
28. Guggenheim S & Flavin M Cystathionine γ -synthase from *Salmonella*. Spectral changes in the presence of substrates. *J. Biol. Chem* 246, 3562–3568 (1971). [PubMed: 4931307]
29. Chang MNT & Walsh CT Stereochemical analysis of γ -replacement and γ -elimination processes catalyzed by a pyridoxal phosphate enzyme. *J. Am. Chem. Soc* 103, 4921–4927 (1981).
30. Guggenheim S & Flavin M Cystathionine γ -synthase. A pyridoxal enzyme catalyzing rapid exchange of β and α hydrogen atoms in amino acids. *J. Biol. Chem* 244, 6217–6227 (1969). [PubMed: 5350958]
31. Krog JS, Espanol Y, Giessing AM, Dziergowska A, Malkiewicz A, Ribas de Pouplana L, & Kirpekar F 3-(3-amino-3-carboxypropyl)-5,6-dihydrouridine is one of two novel post-transcriptional modifications in tRNALys(UUU) from *Trypanosoma brucei*. *FEBS J* 278, 4782–4796 (2011). [PubMed: 22040320]
32. Nishimura S, Taya Y, Kuchino Y, & Oashi Z Enzymatic synthesis of 3-(3-amino-3-carboxypropyl)uridine in *Escherichia coli* phenylalanine transfer RNA: transfer of the 3-amino-acid-3-carboxypropyl group from S-adenosylmethionine. *Biochem. Biophys. Res. Commun* 57, 702–708 (1974). [PubMed: 4597321]
33. Ikegami F, Sakai R, Ishikawa T, Kuo YH, Lambein F, & Murakoshi I Biosynthesis in vitro of 2-(3-amino-3-carboxypropyl)-isoxazolin-5-one, the neurotoxic amino acid in *Lathyrus odoratus*. *Biol. Pharm. Bull* 16, 732–734 (1993). [PubMed: 8401413]
34. Taya Y, Tanaka Y, & Nishimura S Cell-free biosynthesis of discadenine, a spore germination inhibitor of *Dictyostelium discoideum*. *FEBS Lett* 89, 326–328 (1978). [PubMed: 566219]
35. Schneider G, Käck H & Lindqvist Y The manifold of vitamin B₆ dependent enzymes. *Structure* 8, R1–R6 (2000). [PubMed: 10673430]
36. Brzovi P, Litzenberger Holbrook E, Greene RC & Dun MF Reaction mechanism of *Escherichia coli* cystathionine γ -synthase: Direct evidence for a pyridoxamine derivative of vinylglyoxylate as a key intermediate in pyridoxal phosphate dependent γ -elimination and γ -replacement reaction. *Biochemistry*, 29, 442–451 (1990). [PubMed: 2405904]
37. Yamagata S Roles of O-acetyl-L-homoserine sulphydrylases in microorganisms. *Biochimie* 71, 1125–1143 (1989). [PubMed: 2517474]

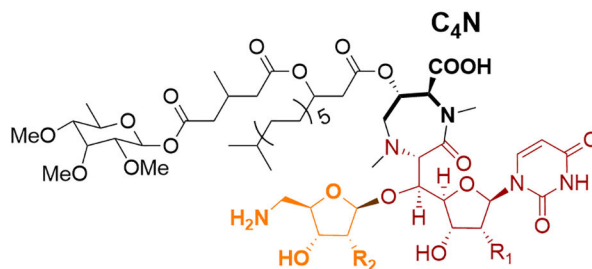
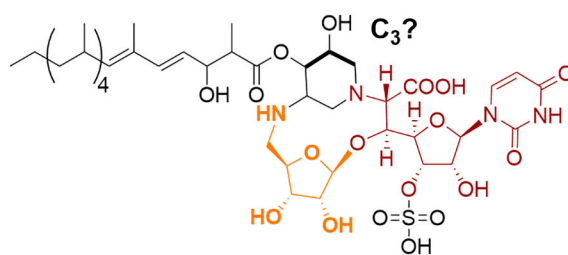
38. Esaki N, Tanaka H, Uemuru S, Suzuki T & Soda K Catalytic action of L-methionine γ -lyase on selenomethionine and selenols. *Biochemistry* 18, 407–410 (1979). [PubMed: 420789]
39. Sato D & Nozaki T Methionine gamma-lyase: The unique reaction mechanism, physiological roles, and therapeutic applications against infectious diseases and cancers. *IUBMB Life* 61, 1019–1028 (2009). [PubMed: 19859976]
40. Omura H, Ikemoto M, Kobayashi M, Shimizu S, Yoshida T & Nagasawa T Purification, characterization and gene cloning of thermostable *O*-acetyl-L-homoserine sulfhydrylase forming γ -cyano- α -aminobutyric acid. *J. Biosci. Bioeng* 96, 53–58 (2003). [PubMed: 16233482]
41. Chiku T, Padovani D, Zhu W, Singh S, Vitivitsky V & Banerjee R H₂S biogenesis by human cystathionine γ -lyase leads to the novel sulfur metabolites lanthionine and homolanthionine and is responsive to the grade of hyperhomocysteinemia. *J. Biol. Chem* 284, 11601–11612 (2009). [PubMed: 19261609]
42. Faulkner JR, Hussaini SR, Blankenship JD, Pal S, Branan BM, Grossman RB, & Schardl CL On the sequence of bond formation in loline alkaloid biosynthesis. *ChemBioChem* 7, 1078–1088 (2006). [PubMed: 16755627]
43. Enders D, Wang C, & Liebich JX Organocatalytic aza-Michael additions. *Chem. Eur. J* 15, 11058–11076 (2009). [PubMed: 19798719]
44. Freedy AM, Matos MJ, Boutureira O, Corzana F, Guerreiro A, Akkapeddi P, Somovilla VJ, Rodrigues T, Nicholls K, Xie B, Jiménez-Osés G, Brindle KM, Neves AA, & Bernardes GJL. Chemoselective installation of amine bonds on proteins through aza-Michael ligation. *J. Am. Chem. Soc* 139, 18365–18375 (2017). [PubMed: 29206031]
45. Xu F, Wu Q, Chen X, Lin X, & Wu Q A single lipase-catalysed one-pot protocol combining aminolysis resolution and aza-Michael addition: An easy and efficient way to synthesise β -amino acid esters. *Eur. J. Org. Chem* 2015, 5393–5401 (2015).
46. Chisuga T, Miyanaga A, Kudo F, & Eguchi T Structural analysis of the dual-function thioesterase SAV606 unravels the mechanism of Michael addition of glycine to an α,β -unsaturated thioester. *J. Biol. Chem* 292, 10926–10937 (2017). [PubMed: 28522606]
47. Kobylarz MJ, Grigg JC, Liu Y, Lee MSF, Heinrichs DE, & Murphy MEP Deciphering the substrate specificity of SbnA, the enzyme catalyzing the first step in staphyloferrin B biosynthesis. *Biochemistry* 55, 927–939 (2016). [PubMed: 26794841]
48. Brotzel F & Mayr H Nucleophilicities of amino acids and peptides. *Org. Biomol. Chem* 5, 3814–3820 (2007). [PubMed: 18004461]
49. Clayden J, Greeves N, & Warren S *Organic Chemistry*, 2nd Ed (Oxford University Press, 2012).nd
50. Shiraishi T, Hiro N, Igarashi M, Nishiyama M, & Kuzuyama T Biosynthesis of the antituberculosis agent caprazamycin: Identification of caprazol-3''-phosphate, an unprecedented caprazamycin-related metabolite. *J. Gen. Appl. Microbiol* 62, 164–166 (2016). [PubMed: 27211833]

References

51. Spork AP, Koppermann S, Dittrich B, Herbst-Irmer R & Ducho C Efficient synthesis of the core structure of muraymycin and caprazamycin nucleoside antibiotics based on a stereochemically revised sulfur ylide reaction. *Tetrahedron Asymmetry* 21, 763–766 (2010).
52. Hirano S, Ichikawa S & Matsuda A Total synthesis of caprazol, a core structure of the caprazamycin antituberculosis antibiotics. *Angew. Chem. Int. Ed* 44, 1854–1856 (2005).
53. Cohen SA & Michaud DP Synthesis of a fluorescent derivatizing reagent, 6-aminoquinolyl-*N*-hydroxysuccinimidyl carbamate, and its application for the analysis of hydrolysate amino acids via high-performance liquid chromatography. *Anal. Biochem* 211, 279–287 (1993). [PubMed: 8317704]
54. Zhang J & Klinman JP High-performance liquid chromatography separation of the (S,S)- and (R,S)-forms of S-adenosyl-l-methionine. *Anal. Biochem* 476, 81–83 (2015). [PubMed: 25681113]
55. Tanaka H, Yamamoto A, Ishida T, & Horiike K Simultaneous measurement of D-serine dehydratase and D-amino acid oxidase activities by the detection 2-oxo-acid formation with reverse-phase high performance liquid chromatography. *Anal. Biochem*, 362, 83–88 (2007). [PubMed: 17254537]



FR-900493 (1)

Caprazamycin B (2) $R_1 = \text{OH}$, $R_2 = \text{OSO}_3\text{H}$ A-90289 B (3) $R_1 = \text{OSO}_3\text{H}$, $R_2 = \text{OH}$ 

Sphaerimycin A (4)

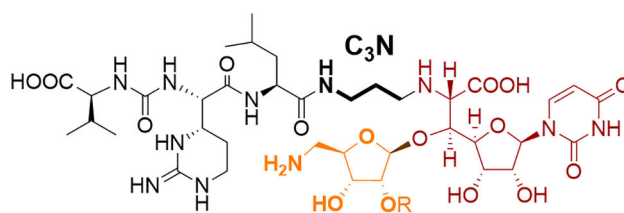
Muraymycin D1 (5) $R = \text{Me}$ Muraymycin D2 (6) $R = \text{H}$

Fig. 1. Structures of representative translocase I inhibitors that contain an *N*-alkylated ADR-GlyU disaccharide core.

The *N*-alkylamine linker (C_3N or C_4N) of unknown biosynthetic origin connects structural components that are unique to each member.

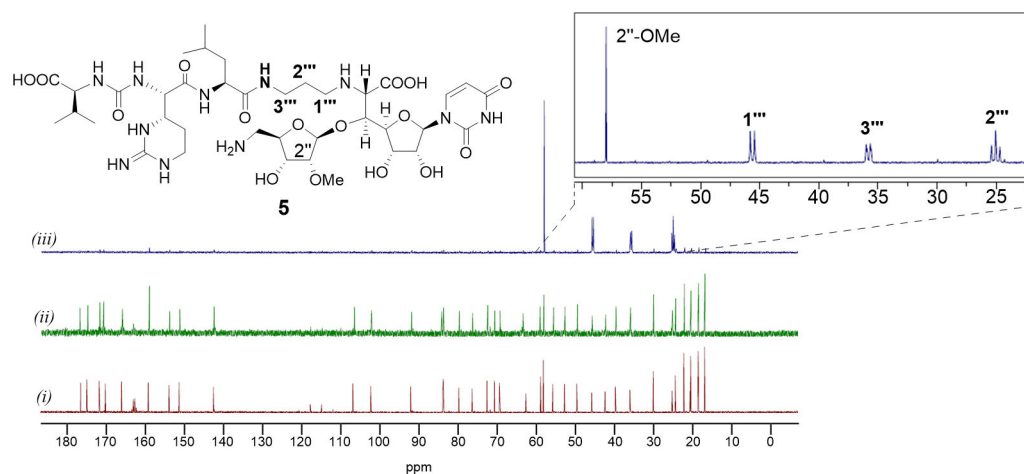


Fig. 2. Spectroscopic analysis of feeding experiments.

^{13}C NMR spectrum (D_2O , 100 MHz) of **5** isolated (i) without feeding (natural isotopic abundance), (ii) following feeding with L- $[^{13}\text{C}_4, ^{15}\text{N}]\text{Asp}$, and (iii) following feeding with L- $[^{13}\text{C}_5, ^{15}\text{N}]\text{Met}$. The inset depicts the zoomed in region of the ^{13}C NMR spectrum to emphasize the splitting pattern of the enriched carbons.

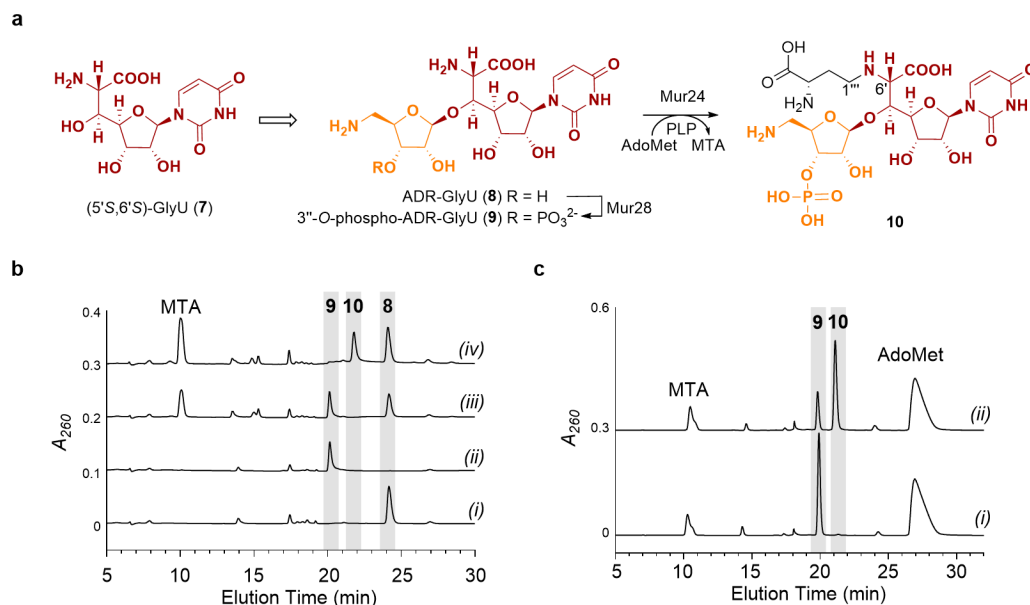


Fig. 3. Functional assignment of Mur24.

a, Structures of known products of enzyme reactions involved in the muraymycin biosynthetic pathway including the proposed reaction catalyzed by Mur24. **b**, HPLC traces of 6-h reactions catalyzed by Mur24 starting with ADR-GlyU (**8**) with (i) exclusion of the phosphotransferase Mur28; (ii) reaction mixture containing ATP and Mur28; (iii) reaction mixture containing ATP, Mur28, and AdoMet with the exclusion of Mur24; (iv) reaction mixture consisting of all the components. A_{260} , absorbance at 260 nm. **c**, HPLC traces of reactions catalyzed by Mur24 starting from **9** with (i) reaction mixture with the exclusion of PLP and (ii) reaction mixture containing all components. A_{260} , absorbance at 260 nm (AU).

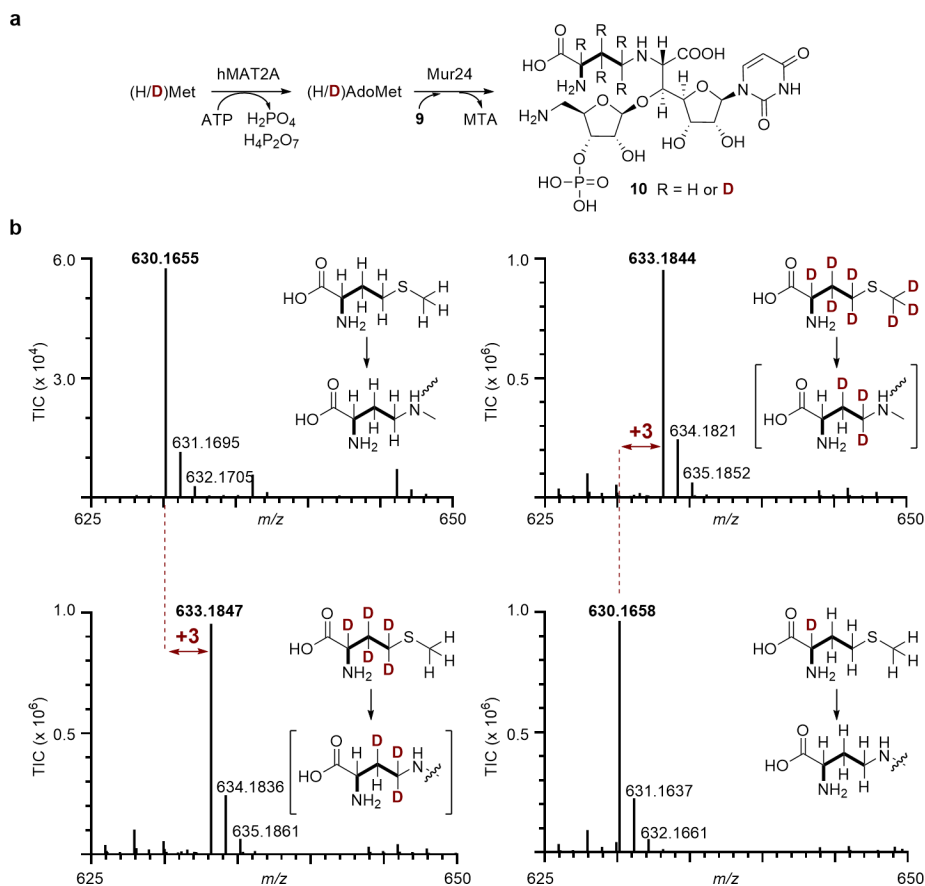


Fig. 4. Isotopic incorporation from L-Met.

a, Enzymatic scheme starting with differentially deuterated L-Met for generating AdoMet isotopologues as a substrate for Mur24. **b**, High resolution mass spectroscopic data for **10** starting with the indicated L-Met isotopologue. The regiochemistry of the incorporated deuteriums in the bracketed products is proposed.

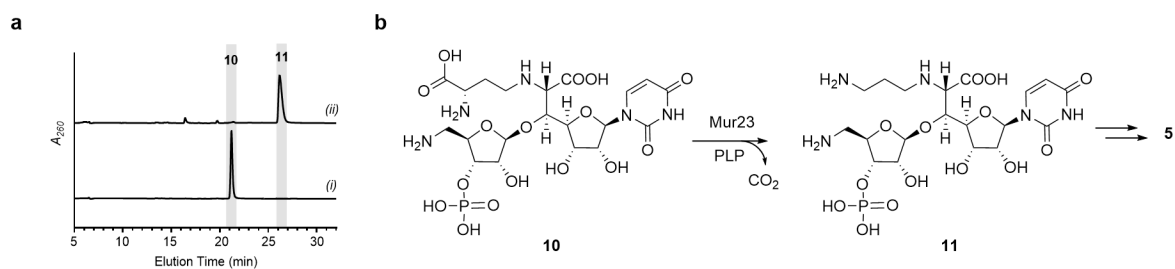


Fig. 5. Functional assignment of Mur23.

a, HPLC traces of (i) control without enzyme and (ii) reaction catalyzed by Mur23 starting from **10** and PLP. A_{260} , absorbance at 260 nm. **b**, Chemical reaction catalyzed by Mur23.

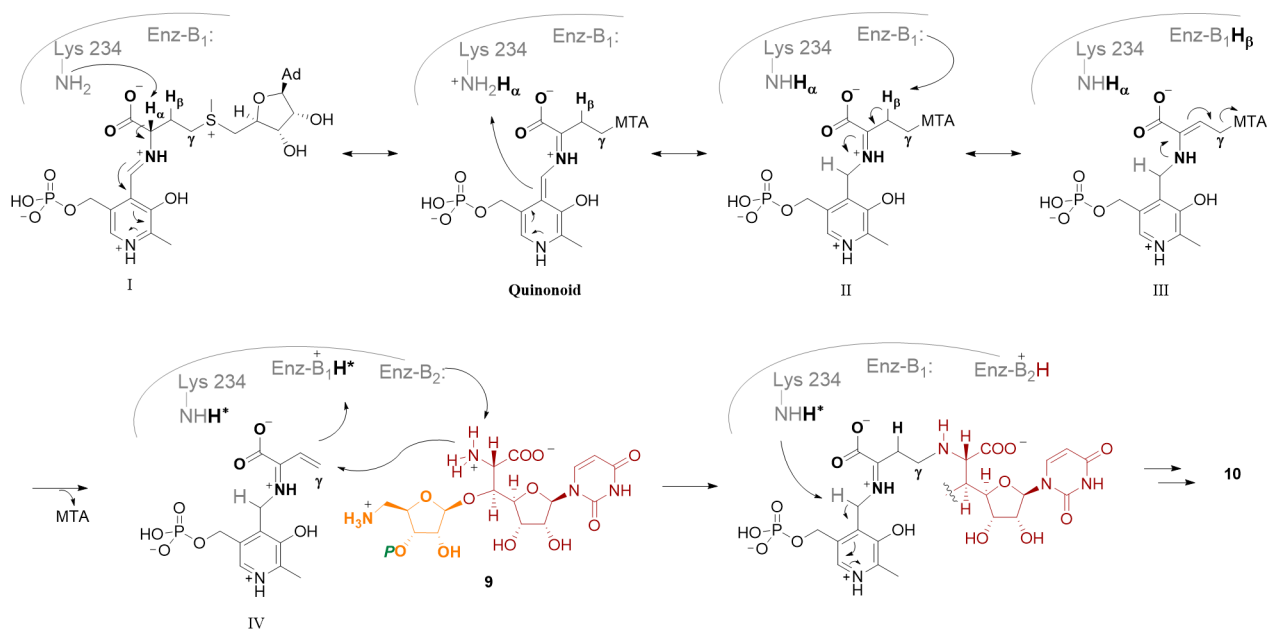


Fig. 6. Putative γ -elimination and γ -addition mechanism for the PLP-dependent AdoMet:9 ABTases.

The asterisk (*) indicates a proton that is different than H_β that is removed from the substrate, which is consistent with isotopic labelling. Following formation of ketimine II, deprotonation at C_β could hypothetically generate an enamine (C_α - C_β double bond), which is not shown, prior to γ -elimination to generate the β,γ -unsaturated ketimine III.